Synthesis of Hierarchically Structured Aluminas under Controlled Hydrodynamic Conditions

Weihua Deng and Brent H. Shanks*

Department of Chemical Engineering, Iowa State University, 2119 Sweeney Hall, Ames, Iowa 50011

Received February 11, 2005. Revised Manuscript Received April 19, 2005

Aluminas having hierarchical bimodal pore structures with regular arrayed macropores interconnected with mesopores were synthesized in a cone/plate apparatus that provided well-defined hydrodynamic conditions. A parametric synthesis study was performed to better understand the synthesis conditions required to form the hierarchical structures. The synthesis experiments demonstrated that the hierarchnical structure could only be formed under limited mixing conditions. The mesoporous structure, which was created by interstitial porosity between boehmite nanoparticles, was formed independently of the macropores and was not significantly impacted by the use of a surfactant, whereas the formation of the macropores required the presence of an alkoxide droplet within the synthesis mixture and the surfactant played no role other than to influence the hydrodynamic conditions during synthesis.

Introduction

Transitional aluminas, which are derived from aluminum hydroxide and oxyhydroxide by thermal treatment,[1] have been extensively used for many decades in industry as catalyst supports,[2] adsorption media and catalysts in processes such as petroleum refining,[3] hydrodesulfurization,[4] and the Claus reaction as well as automotive emission control.[5,6] The discovery of the supramolecular templating technique[7,8] made possible the synthesis of alumina with unique and promising textural properties relative to traditional alumina, which has the potential to further extend its industrial applications. While their synthesis has proven more problematic than their silica analogues, a number of mesostructured alumina synthesis strategies using either ionic or nonionic templating methods have been reported in which the pore diameter can be tuned to a desired dimension.[9−14]

While pore diameter is an important property dictating the mass transfer characteristics of mesoporous alumina, the pore length also plays an important role in mass transfer. The pore length in these materials is largely determined by the morphology of the mesoporous particle. As such, morphology control of mesoporous materials has received increasing attention. A number of studies have demonstrated synthesis methods for mesoporous silica with morphology control, resulting in structures that include particle shapes ranging from spheres to needles to nanotubes.[15−21] Relative to the morphology control achieved with mesoporous silica materials only a few alumina analogues have been reported.[22]

We recently reported the "one-pot" synthesis of a novel macropore/mesopore hierarchically structured alumina in which the alumina particles had parallel arrays of macropores interconnected with mesopores.[23] These materials are interesting for their potential use in catalysis and adsorption applications due to the enhanced access to the mesopores as provided by the regularly arrayed macropores. After our report several groups have reported similar structures for other metal oxides. Su and co-workers have reported the surfactant-mediated and surfactant-free synthesis of hierar-

* Corresponding author. Telephone: 515-294-1869. Fax: 5151-294-2689. E-mail: bshanks@iastate.edu.

(1) Wefers, K.; Misra, C. *Oxide and Hydroxide of Aluminum*; Alcoa Technical Paper No. 19, 1987.
(2) Braunstrin, P.; Kin, Kormann, H. P.; Meyer-Zaika, W.; Pugin, R.; Schmid, G. *Chem. Eur. J.* **2000**, *6*, 4637.
(3) Mirsa, C. *American Chemical Society monograph, Vol. 184: Industrial alumina chemicals*; American Chemical Society: Washington, DC, 1986.
(4) Oberlander, R. K. In *Applied Industrial Catalysis Vol. 3*; Leach, B. E., Ed.; Academic Press: London, 1984.
(5) Tylor, K. C. *Catal. Rev.-Sci. Eng.* **1993**, *35*, 457.
(6) Belton, D. N.; Tylor, K. C. *Cur. Opin. Solid State Mater. Sci*. **1999**, *4*, 97.
(7) Kresge, C. T.; Leonowicz, M. E.; Roth, W. J.; Vartuli, J. C.; Beck, J. S. *Nature* **1992**, *359*, 710.
(8) Beck, J. S.; Vartuli, J. C.; Roth, W. J.; Leonowicz, M. E.; Kresge, C. T.; Schmitt, K. D.; Chu, C. T-W.; Olson, D. H.; Sheppard, E. W.; McCullen, S. B.; Higgins, J. B.; Schlenker, J. L. *J. Am. Chem. Soc.* **1992**, *114*, 10834.
(9) Tanev, T. P.; Pinnavaia, T. J. *Science* **1995**, *267*, 865.
(10) Bagshaw, S. A.; Pinnavaia, T. J. *Angew. Chem., Int. Ed. Engl*. **1996**, *35*, 1102.
(11) Vaudry, F.; Khodabandeh, S.; Davis, M. E. *Chem. Mater*. **1996**, *8*, 1451.
(12) Cabrera, S.; Haskouri, J. E.; Alamo, J.; Beltrán, A.; Beltrán, D.; Mendioroz, S.; Macros, M. D.; Amorós, P. *Adv. Mater*. **1999**, *5*, 371.
(13) Liu, X.; Wei, Y.; Jin, D.; Shih, D. *Mater. Lett*. **2000**, *42*, 143.
(14) Valange, S.; Guth, J.-L.; Kolenda, F.; Lacombe, S.; Gabelica, Z. *Microporous Mesoporous Mater*. **2000**, *35*−*36*, 597.
(15) Schacht, S.; Huo, Q.; Voigt-Martin, I. G.; Stucky, G. D.; Schûth, F. *Science* **1996**, *273*, 768.
(16) Huo, Q.; Feng, J.; Schûth, F.; Stucky, G. D. *Chem. Mater.* **1997**, *9*, 14.
(17) Huo, Q.; Zhao, D.; Feng, J.; Weston, K.; Buratto, S. K.; Stucky, G. D.; Schacht, S.; Schûth, S. F. *Adv. Mater.* **1997**, *9*, 974.
(18) Zhang, W.; Pauly, T. R.; Pinnavaia, T. J. *Chem. Mater.* **1997**, *9*, 2491.
(19) Pauly, T. R.; Liu, Y.; Pinnavaia, T. J.; Billinge, S. J. L.; Rieker, T. P. *J. Am. Chem. Soc.* **1999**, *121*, 8835.
(20) Cai, Q.; Luo, Z.; Pang, Z.; Fan, Y.; Chen, X.; Cui, F. *Chem. Mater*. **2001**, *13*, 258.
(21) Lin, H.; Mou, C. *Science* **1996**, *273*, 765.
(22) Luo, Q.; Li, L.; Xue, Z.; Zhao, D. In *Studies in Surface Science and Catalysis, Vol. 129*; Sayari, A., Jaroniec, M., Pinnavaia, T. J., Eds.; Elsevier Science: Amsterdam, 2000; p 37.
(23) Deng, W.; Toepke, M. W.; Shanks, B. H. *Adv. Funct. Mater*. **2003**, *13*, 61.

10.1021/cm050315j CCC: $30.25
Published on Web 05/17/2005

chically structured metal oxides such as zirconia, alumina, and aluminosilicate.[24−29] Mann and co-workers have demonstrated the template-free synthesis of ordered macroporous titania.[30]

In our initial report a preliminary study of the synthesis parameter space was explored. The hierarchical structures were found to form quite rapidly, making direct observation of the synthesis progression difficult.[23] Importantly, it was found that the hydrodynamic environment present during the synthesis had a significant effect on the formation of the unique particle morphology. To provide a well-controlled hydrodynamic environment, a cone/plate apparatus[31−33] was designed and adopted as the synthesis reactor in the current work. Under these carefully controlled hydrodynamic conditions, a systematic study examining the effect of synthesis conditions on the formation of the hierarchical alumina structure was performed. The results from the parametric synthesis study were then used to discuss possible mechanisms for the formation of the hierarchical structure.

Experimental Section

Aluminum *sec*-butoxide (97%) and amine surfactants (dodecyl-, cetyl-, and octadecyl-trimethylamonium bromide) were used as purchased from Aldrich (USA). Also used in the study was a nonionic poly(ethylene oxide)/polypropylene oxide triblock copolymer surfactant (Pluronic L64, BASF, USA), ethanol (100%, Fisher Scientific, USA), and deionized water.

All syntheses were conducted in a cone/plate apparatus (CPA) as shown in Figure 1, which consisted of a small angle (around 5°) rotating cone within a cylindrical vessel. The apparatus, which is equivalent in structure to a cone/plate viscometer, allowed the synthesis to be conducted in a well-controlled and uniform shear field. The ratio of the centrifugal to viscous force acting on the fluid in the CPA can be characterized using a dimensionless parameter R, which is a Reynolds number,[31]

$$R = r^2\omega\alpha^2/12\nu$$

where r is the radial distance from the cone center to the inlet of a unidirectional valve at the bottom of the vessel, ω the angular velocity of the cone, α the cone angle in radians, and ν the kinematic viscosity of the fluid.

A typical synthesis was performed by first introducing the surfactant, water, and ethanol mixture into the CPA where it was mixed under stirring conditions for 10 min. Then, the aluminum tri-*sec*-butoxide was directly introduced into the system by injection at a rate of about 1 mL/min through a unidirectional valve of 1/16 in. diameter installed on the bottom of the vessel. The mixture was aged under a constant cone velocity for 60 min. The sample was retrieved by filtration and washed by water and ethanol thoroughly and dried in air at ambient temperature for about 12 h. The samples were calcined for 5 h in flowing air at 500 °C using a temperature ramp rate of 2 °C/min from room temperature to that temperature. The synthesis factors evaluated in the parametric study were cone velocity, surfactant choice, water/ethanol ratio, and cosolvent selection. Shown in Table 1 is a representative set of the range of parameters used for the study.

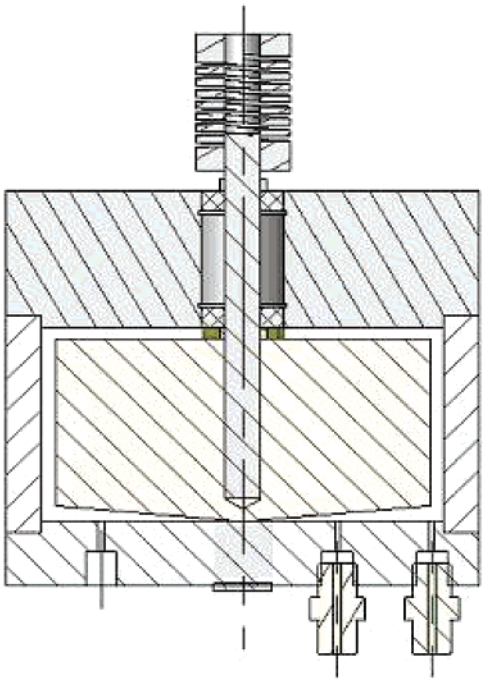

Figure 1. Schematic of the cone/plate apparatus.

Powder X-ray diffraction (XRD) patterns were acquired by an X_1 advanced diffraction system (Scintag, Inc.) using a Cu Kα radiation source ($\lambda = 0.154$ nm). Low-angle X-ray diffraction with a 2θ range of 0.5−10° was used to investigate the mesoporosity of the materials and wide angle scans were performed within a 2θ range of 5−85° to determine the crystallinity of the materials. The surface area (SA) and pore size distribution were measured using a Micromeritics ASAP 2000. The SA was determined using the Brunauer−Emmett−Teller (BET) method and the Barrett−Joyner−Helenda (BJH) method was used to determine pore volume (PV) and pore size distribution. Sample preparation included degassing at 90 °C for 1 h followed by 200 °C for at least 4 h. SEM images were taken using a JSM-840 scanning microscope (JEOL Inc.) with gold-coating sample preparation. For the transmisson electron microscopy (TEM) studies, thin sections of samples (60−80 nm) embedded in epoxy resin were obtained using ultramicrotomy. The resulting sample was examined with a Philips model CM-30 TEM operated at 300 kV. TGA and DTG curves were recorded using a Perkin-Elmer TGA7 thermogravimetric analyzer with a 10 °C/min temperature ramp rate and a purging gas of dry air.

Results

Shown in Table 1 are the parametric synthesis conditions for a representative set of aluminas synthesized for the study. The table also provides the textural properties measured for the resulting materials using BET characterization and SEM observation. For a given synthesis that resulted in particles with macropores, the macropores were sometimes only found in a portion of the sample particles. The column labeled "occurrence" denotes the percentage of the total alumina particles that were found to contain macropores as deter-

(24) Yuan, Z.; Vantomme, A.; Leonard, A.; Su, B. *Chem. Commun*. **2003**, 1559.
(25) Yuan, Z.; Ren, T.; Su, B. *Adv. Mater*. **2003**, *15*, 1462.
(26) Blin, J.; Leonard, A.; Yuan, Z.; Gigot, L.; Vantomme, A.; Cheetham, A. K.; Su, B. *Angew. Chem., Int. Ed.* **2003**, *42*, 2872.
(27) Ren, T.; Yuan, Z.; Su, B. *Langmuir* **2004**, *20*, 1531.
(28) Yuan, Z. Y.; Ren, T. Z.; Vantomme, A.; Su, B. *Chem. Mater*. **2004**, *16*, 5096.
(29) Leonard, A.; Su, B. *Chem. Commun*. **2004**, 1674.
(30) Collins, A.; Carriazo, D.; Davis, S. A.; Mann, S. *Chem. Commun.* **2004**, 568.
(31) Sdougos, H. P.; Bussolari, S. R.; Dewey, C. F. *J. Fluid Mech*. **1984**, *138*, 379.
(32) Einav, S.; Dewey, C. F.; Hartenbaum, H. *Exp. Fluids* **1994**, *16*, 196.
(33) Grad, Y.; Einav, S. *Exp. Fluids* **2000**, *28*, 336.

Table 1. Sample Preparation Conditions and Characterization Results

ID	Co−S/S (V/V)	$C_{Surfactant}$ mM	cone speed rpm	R	occurrence %	MMPD nm	SA m^2/g	PV cm^3/g	MPD[a] A
1	0.25	0.022	100	8.8	90	500	430	0.56	50
2	0.25	0.022	200	18	90	650	410	0.5	47
3	0.25	0.022	500	44	95	850	370	0.51	53
4	0.25	0.022	750	66	25	1000	380	0.52	52
5	0.25	0.022	100	8.8	0	N/A	340	0.36	40
6	0.25	0.014	100	7.9	90	600	440	0.44	38
7	0.25	0.014	500	39	90	850	420	0.41	38
8	0.25	0.014	1000	79	90	1000	370	0.42	44
9	0.25	0.022	100	11	95	550	400	0.46	44
10	0.25	0.022	100	10	85	750	360	0.4	42
11	0.67	0.022	100	7.4	75	1000	470	0.91	75
12	1.5	0.022	100	6.9	25	600	420	0.56	51
13	4	0.022	100	7.7	0	N/A	440	0.56	48
14	0.25	0.022	100	10	85	1000	470	0.49	39
15	0.25	0.022	100	14	90	700	420	0.51	46
16	0	0	100	17	90	750	460	0.49	40
17	0	0	200	34	90	850	480	0.46	37
18	0	0	500	86	90	1200	390	0.43	41
19	0	0	750	130	0	N/A	310	0.32	41

[a] Apparent MPD since "ink-bottle" pore morphology dominates.

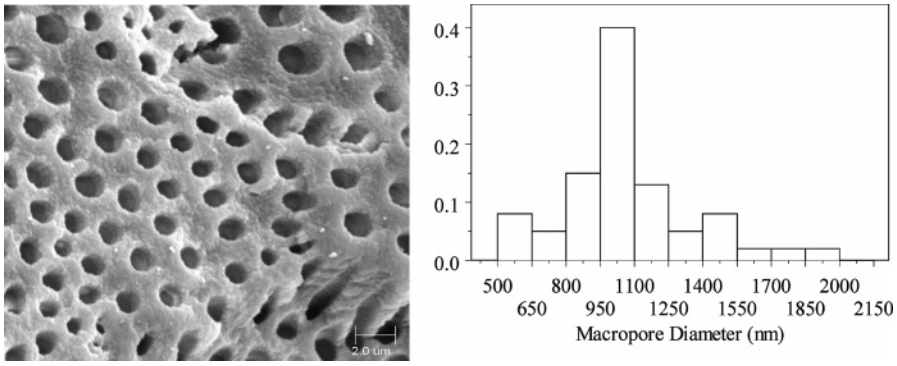

Figure 2. Representative SEM image from sample 4 and its macropore size distribution (right).

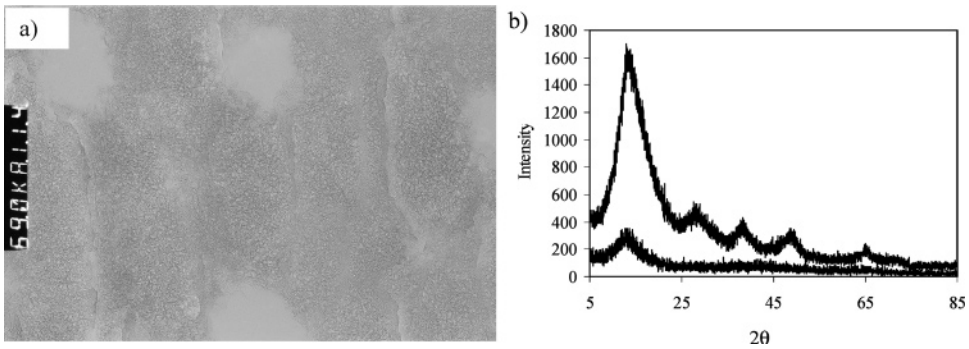

Figure 3. (a) TEM image for sample 2 (~700 nm macropores); (b) wide-angle XRD scans for sample 2 with 60 min of aging (above) and 10 min of aging (below).

mined by SEM. Although the macropore diameter varied under different synthesis conditions in an interval between 500 and 1500 nm, it was found to have a relatively narrow size distribution for a specific sample. Shown in Figure 2 is a representative SEM image for sample 4 and the resulting macropore size distribution obtained from analysis of the image. For this sample, a median macropore diameter (MMPD) of about 1000 nm was determined. The MMPDs for the materials containing macropores are also included in Table 1.

Low-angle XRD patterns for all samples gave a broad peak between 2θ of 1 and 3°, indicating the existence of a mesostructure. The intensity of this peak was found to increase following calcination of the samples. A TEM image for a sample prepared under sample 2 conditions is given in Figure 3a. An irregular mesopore motif can be seen in the walls of the material between the macropores, which are about 700 nm in size. Shown in Figure 3b are wide angle XRD patterns for representative materials synthesized under sample 2 conditions at two different aging times. Sample 2, which was aged for 60 min, had discrete peaks that could be assigned to the boehmite structure.[34] In contrast, the sample that was only aged for 10 min did not display significant boehmite structure as measured by XRD. The

(34) Hicks, R. H.; Pinnavaia, T. J. *Chem. Mater*. **2003**, *15*, 78.

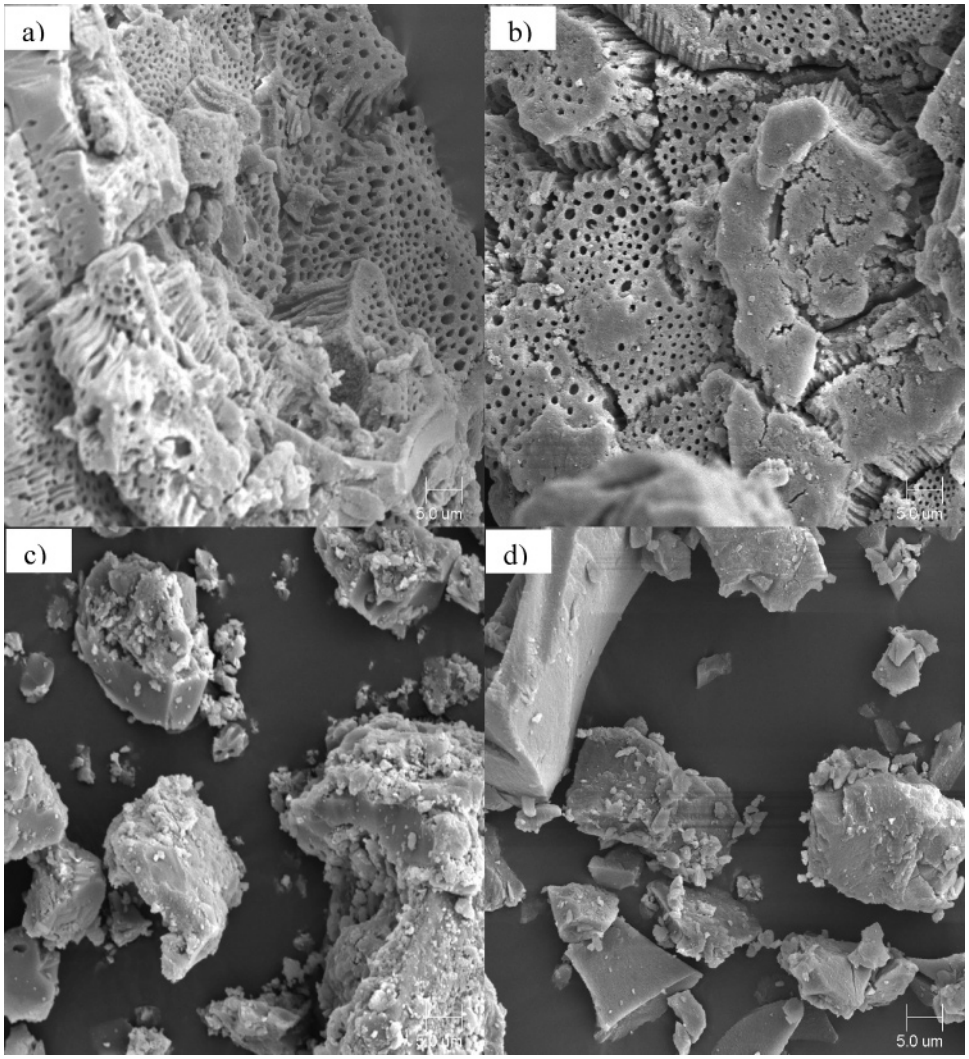

Figure 4. SEM images (5 μm scale bar): (a) sample 1, (b) sample 3, (c) sample 4, and (d) sample 5.

XRD result for the typical synthesis was inconsistent with surfactant-templated mesoporous aluminas that are amorphous, but was consistent with mesoporous materials resulting from the assembly of nanoparticles. The presence of the boehmite structure, which was seen across the entire set of hierarchical materials, in conjunction with the TEM suggested that the macropores in the material were interconnected with networks of mesopores created by interstitial voids between crystalline boehmite nanoparticles.

Samples 1−5 were synthesized under the base water/ethanol/surfactant concentrations used in the previous study.[23] However, the mixing conditions used in each synthesis were varied. For samples 1−4, the cone speed was increased from 100 to 750 rpm corresponding to *R*-values of 8.8 to 66, whereas for sample 5 the aluminum alkoxide was first mixed with the *sec*-butanol, which ensured complete dissolution of the aluminum alkoxide, and then the mixture was introduced to the CPA. Shown in Figure 4 are representative SEM images for samples 1, 3, 4, and 5. As seen previously, the hydrodynamic conditions had a strong effect on particle morphologies. For samples 1−3 regular parallel arrays of macropores having relatively uniform size were seen quite clearly in nearly every alumina particle. The macropores were orthogonal to the face of the particles and were found from SEM images to either pass completely through the particle or to be closed off at one side after passing through most of the particle. Increasing the strength of the shear force that was manifest in higher *R*-values resulted in suppression of the macroporous structure. The *R*-value of 66 used in sample 4 gave only a limited number of particles (25%) having any macropores and those macropores that were present were significantly more irregular than in samples 1−3. No macropores were observed when *R*-values of greater than 100 were used. In addition to ultimately causing complete suppression of the macropores, increasing the shear force appeared to cause the MMPD to increase. When the aluminum alkoxide was introduced in a dispersed state as in sample 5 rather than directly as droplets, no macropores were observed in the resulting alumina particles. Therefore, the introduction of an aluminum alkoxide droplet into the synthesis mixture was clearly required for the formation of macropores.

The N_2 adsorption−desorption isotherm plots and pore size distribution (PSD) curves for the aluminas synthesized under different mixing conditions are shown in Figure 5. Each of the materials had a type IV isotherm with a fairly broad H2 hysteresis loop between relative pressures 0.4 and 0.8, indicating a distribution of pores in the mesoporous range.[35]

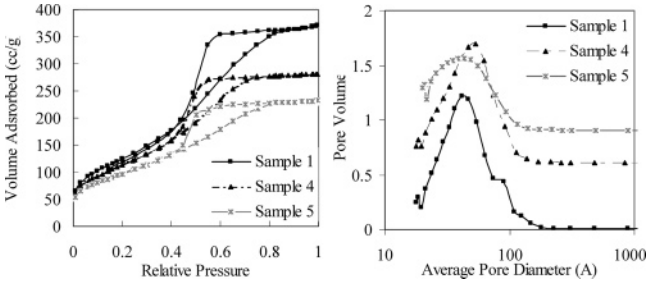

Figure 5. N_2 adsorption−desorption isotherm plots and pore size distribution curves.

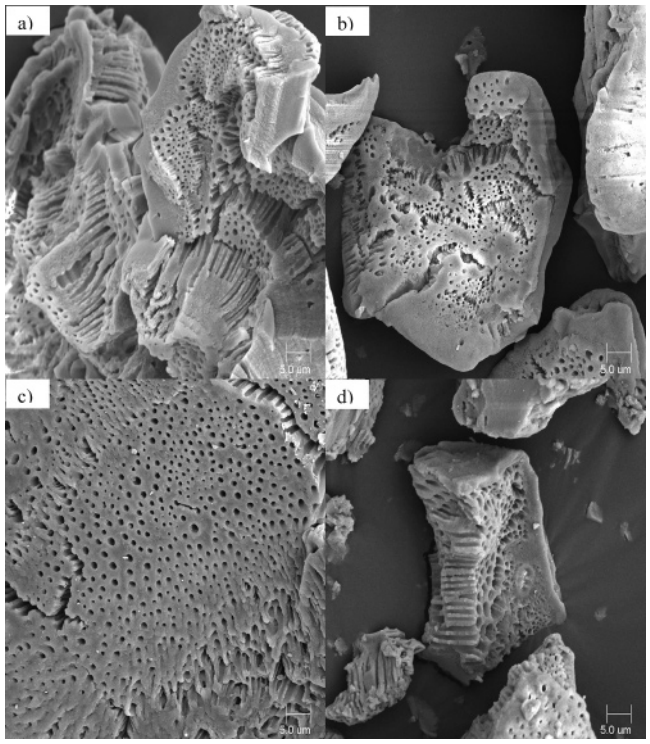

Figure 6. SEM images (5 μm scale bar) for the Pluronic L64 samples, (a) sample 6 and (b) sample 7, and for the aluminum alkoxide/water only samples, (c) sample 16 and (d) sample 17.

The broad hysteresis loop suggests that these mesopores are not cylindrical but exist as a network of pores containing "ink-bottle" pores.[35] The PV and median pore diameter (MPD) of samples 1−4 were effectively independent of the mixing conditions. In contrast, sample 5, which had the aluminum alkoxide that was first dissolved in butanol, gave lower values for the PV and MPD.

To examine the role of the surfactant on the formation of the hierarchical structures, syntheses were performed with other surfactants. Samples 6−8 were synthesized under varying mixing conditions using the nonionic Pluronic L64 surfactant rather than the ionic cetyltrimethylammonium bromide (CTAB) surfactant. The textural properties for these samples are given in Table 1 and the SEM images for samples 6 and 7 are given in Figures 6a and 6b, respectively. As can be seen from the micrographs, the macroscopic particle morphologies for these samples were similar to that of the base case. For all three samples nearly all of the particles contained macroporous structure. As with the

(35) Groen, J. C.; Perez-Ramirez, J. *Appl. Catal., A* **2004**, *268*, 121.

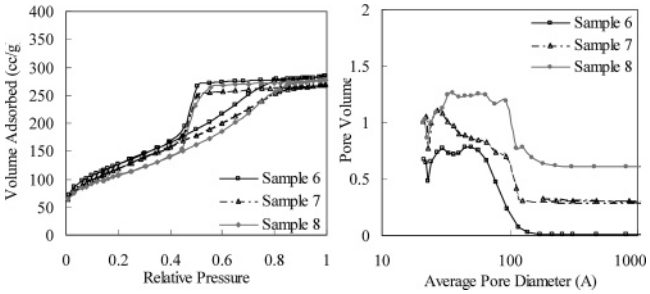

Figure 7. N_2 adsorption−desorption isotherm plots and pore size distribution curves for the Pluronic L64 samples.

previous set, increasing the shear rates such that the *R*-value increased above about 100 eliminated the formation of macropores in the particles. An upward trend in MMPD again was found to correspond with increasing *R*-values.

While the macroporous structure was similar for materials synthesized with either CTAB or Pluronic L64 under comparable mixing conditions, the mesoporous structure was influenced by the choice of surfactant. The samples synthesized in the presence of Pluronic 64 had lower PV and MPD than those in which CTAB was used. The difference in PV and MPD was also manifest in the pore size distribution, as can be seen from comparing the pore size distributions in Figures 7 and 5. The materials made in the presence of Pluronic L64 had significantly broader pore size distributions and sharper decreases on the desorption branch, indicating an "ink-bottle" pore structure. Despite the difference in mesoporous structure, both the Pluronic L64 and CTAB-based samples were found from wide-angle XRD to contain boehmite.

Syntheses were also performed with ionic surfactants having longer carbon chain length. Samples 9 and 10 correspond to materials made in the presence of dodecyltrimethylammonium and octadecyltrimethylamonium bromide, respectively, at *R*-values of about 10. In these samples nearly all of the particles contained macropores. The textural properties determined from BET analysis were similar to those of the materials made in the presence of CTAB. From the alternative surfactant work, the response of the mesopore structure to the choice of surfactant was not correlated, as would be expected if the mesopores were being created by a templating-type interaction, but was consistent with the results reported for nanoparticle assembly in aluminas.[32]

The role of the cosolvent in the formation of the hierarchical structure was examined by varying the ethanol/water ratio as well as substituting other solvents for the ethanol. All of the samples were synthesized at *R*-values of about 10. Samples 1 and 11−13 provided a comparison of the effect of the ethanol/water ratio. Representative SEM images for this set of samples are shown in Figure 8. Two notable regions can be seen in the micrographs of the samples. The macropores can be seen on one face of the particle and the other face of the particle contained no macropores. As reported in the macroporous titania system,[28] many of the macroporous alumina particles in the current work appeared to have macropores that did not extend completely through the particle. However, there were also other particles in which the macropores did transverse the entire particle. As a

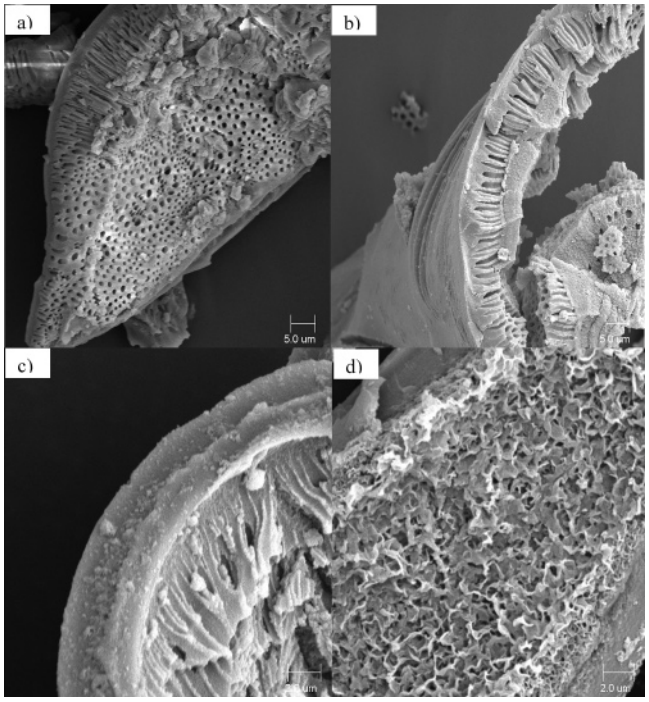

Figure 8. SEM images (5 μm scale bar for a and b, 2 μm scale bar for c and d) for ethanol/water ratio samples: (a) sample 1, (b) sample 11, (c) sample 12, and (d) sample 13.

qualitative observation from the ethanol/water ratio samples, the thickness of the macropore-free portion of the particle appeared to increase with the increasing of ethanol/water volumetric ratio. Increasing the ethanol/water ratio from 0.25 to 0.67 maintained the macropores in most of the particles, but a further increase to 1.5 (sample 12) diminished the particles containing macropores to 25%. The formation of macropores was completely suppressed when an ethanol/water ratio of 4 was used. With the exception of the PV for sample 11, the characteristic textural properties as determined from N_2 adsorption/desorption for the ethanol/water ratio samples were similar.

Surface areas of higher ethanol/water ratio samples were not very different from that of the base case synthesized samples; however, PV and pore structure of these samples varied significantly, as can be seen in Table 1. Unlike isotherms shown previously, the ethanol-rich samples had N_2 adsorption−desorption isotherms with distinctly different shape. Each isotherm had two hysteresis loops: one between relative pressure of 0.4 and 0.85 and another in the higher relative pressure region. The first hysteresis loop, which is a type H2, can be attributed to similar mesporous structure as in the other samples and the second could be assigned to the existence of textural mesoporosity in the material.[34]

In previous initial screening work, *sec*-butanol and acetone were used to investigate the cosolvent effect on the formation of hierarchically structured aluminas.[23] Since the heterogeneous mixing conditions used in that synthesis were effectively in the transition region to shear rates above those able to sustain formation of macropores, the effect of using *sec*-butanol and acetone as the cosolvents on the formation of macropores was re-examined under controlled mixing at low *R*-values. These materials correspond to samples 14 and 15 for *sec*-butanol and acetone, respectively. As can be seen

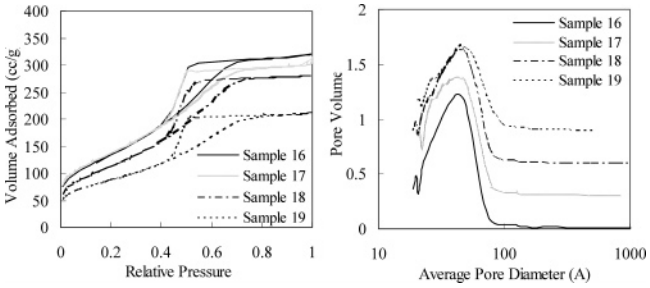

Figure 9. N_2 adsorption−desorption isotherm plots and pore size distribution curves for the aluminum alkoxide/water only samples.

from Table 1, these materials had macropores and textural properties that were the same as when ethanol was used as the cosolvent. Therefore, when the synthesis of the hierarchical alumina was performed within a controlled mixing regime, the choice of cosolvent had no effect on the morphologies of the resulting powders.

Since macropore formation appeared to be independent of the surfactant or cosolvent used, syntheses were performed in the absence of either a surfactant or cosolvent. The textural properties of these materials (samples 16−19), which were made under varying mixing conditions, are given in Table 1. The presence of regular arrays of macropores can be clearly seen in representative SEM images for samples 16 and 17 as seen in Figures 6c and 6d. As with the surfactant-containing synthesis, the formation of macropores was suppressed in the surfactant-free synthesis when mixing conditions were increased to *R*-values of above 100. Due to the lower viscosity of the synthesis mixture, lower cone speeds were required when a surfactant was not used. The consistent *R*-value required for macropore formation indicated that the Reynolds number parameter could be used to define the hydrodynamic conditions that would yield a hierarchically structured material. The trend of increasing MMPD with increasing *R*-value was seen in samples 16−18 as it was in surfactant-mediated syntheses at varying mixing conditions.

While the textural properties of the samples synthesized without surfactant or cosolvent were similar to those measured for the base case materials, the PVs for samples 16−18 were somewhat lower than for samples 1−4. Shown in Figure 9 are the N_2 adsorption−desorption isotherm plots and PSD curves for samples 16−19. The pore size distributions for these samples were similar to those for the base case materials. Upon comparing all of the samples, the cosolvent appeared to have no impact on the structure of the mesopores. However, the choice of surfactant (ionic or nonionic) as well as the use of a surfactant was found to have some effect on defining the size and morphology of the resulting mesoporous structure.

Samples synthesized with and without the use of a surfactant were tested in the TGA following the 12 h drying period. Similarly shaped TGA curves were observed for both types of samples with significant weight losses only in the 70−120 °C region, which could be attributed to the loss of physisorbed water, and the 300−500 °C region, which was due to dehydroxylation. If the surfactant was present after the water and ethanol washing procedure, it would cause a

weight loss centered at about 300 °C.[36] The lack of a significant weight loss at that temperature indicated that no significant surfactant was left after the washing procedure, which is inconsistent with the ionic surfactant serving a templating role. The high water loss levels observed, particularly for samples 1 and 6, were consistent with "ink-bottle" type restricted pores that would retain water even after ethanol washing.

Discussion

The experimental results demonstrated that aluminas with pores at two distinct length scales could be produced from a defined range of synthesis conditions. Additionally, the set of conditions used in the study would strongly suggest that the formation of these two different characteristic pore morphologies were decoupled since they could be individually manipulated by the choice of synthesis condition. For example, the macropore formation was strongly influenced by changes in the hydrodynamic environment for a given synthesis composition, but the mesoporous structure was unaffected, whereas the choice of surfactant or the use of no surfactant affected the mesoporous structure while not affecting the macroporous structure at a fixed *R*-value. Therefore, it is possible to discuss the formation mechanisms for the two types of pores serially.

The formation mechanism for the mesoscale structure in the aluminas reported here would appear to be similar to that proposed by Hicks and Pinnavaia, where the mesopores correspond to the interstitial voids between boehmite nanoparticles.[34] As with the N_2 adsorption−desorption isotherms for their materials, broad hystersis loops were observed in the mesopore size range, indicating a network of interconnected pores that are not cylindrical, but have restrictions leading to "ink-bottle" shaped pores. The presence of boehmite particles was clearly evident by the XRD patterns, which became more pronounced with increased aging time.

Previous work with the synthesis of mesostructured aluminas demonstrated that the choice of mediating surfactant influenced the resulting mesostructure with ionic and nonionic surfactants, yielding different nanoparticle aggregation.[34,37] Unlike in the templating mechanism, change in the chain length of the ionic amine surfactant used in the synthesis was reported to have no impact on the resulting mesopore structure. As demonstrated by samples 1, 9, and 10 that were synthesized with different carbon chain length ionic surfactants, this same invariance was observed in these materials. The change to a nonionic surfactant or the elimination of a surfactant entirely from the synthesis did lead to changes in the mesoporous structure, further demonstrating that the surfactant did influence the aggregation of the boehmite nanoparticles.

While the mesoporous structure formation mechanism in the materials appeared to be consistent with previous reports, the macropore formation mechanism has not been previously resolved. The current set of parametric syntheses under well-defined hydrodynamic conditions demonstrates synthesis conditions necessary for the macroporous structure to form. Critically important is the presence of an alkoxide droplet in the synthesis solution. As demonstrated in sample 5, the pre-dispersal of the alkoxide in anhydrous alcohol completely suppressed macropore formation. In addition, high Reynolds number (*R*-value), which would cause more rapid breakup of the alkoxide droplets, also suppressed macropore formation. The need for an intact alkoxide droplet is also consistent with the rapid formation of the macroporous structure, which would not occur with a slower assembly process such as that seen with templated mesoporous silicas.

The surfactant did not appear to play any direct role in the macroporous structure as demonstrated by generation of macropores even in the absence of any surfactant. Indirectly, the surfactant influenced the macropores by changing the hydrodynamic environment. Due to the increased solution viscosity upon inclusion of the surfactant, a larger range of mixing speeds could be employed that would still stay within the envelope of Reynolds numbers required for macropore formation. As such, a synthesis being performed in the presence of a surfactant in a standard flask with heterogeneity of mixing conditions would be more likely to form macropores than without the surfactant since the range of Reynolds numbers being accessed would be attenuated. The lack of direct surfactant role in the synthesis of the macroporous structure was consistent with that reported by Mann and coworkers[30] and Su et al.[28,29]

Due to the rapid formation of the macropores, the porous structure can be attributed to a kinetically accessed framework rather than an equilibrated structure. Therefore, the rates of hydrolysis of the aluminum alkoxide and condensation of the aluminate are critically important. The results in the current work and previous studies clearly demonstrate that the hydrolysis rate must be within a specific range to form the macropores. A commonality between our alumina macroporous structures and those reported for titania and zirconia was that highly reactive alkoxide precursors were required. When the hydrolysis rate was slowed by dilution with the alcohol cosolvent, the macropores did not form. As shown in our prior paper, increasing the hydrolysis rate by increasing the synthesis temperature also suppressed macropore formation.[23]

From the results, the overall formation of the hierarchical structures appears to occur via hydrolysis and condensation on the external surface of the alkoxide droplets. Once the alumina particles reach a certain size range, they detach from the droplet surface, thereby exposing a "fresh" alkoxide surface to begin the process again. The use of an alkoxide that readily hydrolyzes ensures that the hydrolysis will occur more rapidly at the surface than dissolution of the alkoxide into the solvent.

The clear requirement for the presence of an alkoxide droplet does not, however, explain the formation of the macropore structure and the rapid rate of macropore structure formation makes direct observation of the formation mechanism difficult. Precedent does exist for the formation of regularly arrayed macroporous metal oxides. The synthesis

(36) Deng, W.; Bodart, P.; Pruski, M.; Shanks, B. H. *Microporous Mesoporous Mater*. **2002**, *52*, 169.
(37) Zhang, Z.; Hicks, R. W.; Pauly, T. R.; Pinnavaia, T. J. *J. Am. Chem. Soc.* **2002**, *124*, 1592.

of hexagonal arrayed macroporous alumina by aluminum anodization has been the subject of extensive studies.[38−40] The striking similarity in organization and length scale of the anodization-derived materials and our materials suggests that some analogies might exist in the formation mechanisms of the materials.

The anodic oxidation of aluminum occurs by placing a voltage on an aluminum substrate to create a current density that drives oxidation of the surface aluminum. During the anodization process three distinct regions exist: the aluminum substrate, the aluminum oxide surface layer, and the acidic electrolyte solution. Growth of the oxide layer is coupled with some dissolution of Al^{3+} into solution. The generation of regularly arrayed porous alumina from the anodic oxidation of aluminum has two important steps, initiation of the hexagonal pattern of the pores on the surface of the aluminum and the propagation of the pores through the aluminum substrate.

Significant debate still exists about the mechanism of the pore initiation with attention largely centered upon the nanoscale morphology of the original aluminum substrate. During initiation of the oxidation, an oxide film forms across the entire surface. The film thickens since oxygen transport through the film and oxidation at the metal−film interface occurs more readily than dissolution of Al^{3+}. As the film reaches a thickness exceeding the height of initial features in the aluminum surface, a regular scalloped pattern develops at the metal−film interface. At this point, a higher local conduction resistance occurs at the ridges of the scallop relative to the valleys. The higher current density in the valleys causes locally enhanced rates of oxidation and dissolution.[41,42] The electrochemical enhancement of the oxidation and Al^{3+} dissolution rates in the hemispherical-shaped valleys that are established in the initiation step leads to propagation of the base of the pore through the aluminum. As the pore propagates, the current density at the base of the pore greatly exceeds that through the wall, leading to the second stage of macropore formation, which is the growth of the pore.

In principle, the hydrolysis and dissolution occurring at the surface of the aluminum alkoxide droplet is analogous to the oxidation and dissolution occurring at the aluminum substrate surface. While the applied voltage provides the driving force for the oxidation reaction, the hydrolysis reaction has a sufficient chemical driving force to proceed rapidly. If a scalloped-type pattern was established at the droplet surface, enhanced rates of hydrolysis and solubilization would be expected in the valleys where the alkoxide/solvent interaface was most exposed. Once the pores initiated, they would propagate toward the alkoxide preferentially to causing any change in the pore walls. After the condensed macroporous alumina particle reached a sufficient size, it would then break off from the alkoxide droplet.

This proposed macropore development mechanism leaves several unanswered questions. As with the anodization process, the cause of the initiation of the macropore array is unclear. Second, as reported in the titania work by Mann and co-workers,[30] many of the macroporous alumina particles contained macropores that did not transverse the entire particle as seen clearly in Figures 8a and 8b.

The macropore-free shell on one side of the particle coupled with the curvature of the particle led Mann and co-workers to propose a formation mechanism that involved initial formation of a mesoporous semipermeable membrane on the outside of the alkoxide droplet. They propose the formation of this membrane restricts the hydrolysis/condensation domain such that the reaction subsequently moves inward. The formation of the macropore channels are attributed to microphase-separated regions of metal oxide and solvent established by flow of the solvent across the membrane to the alkoxide interface. This proposed formation mechanism for the macroporous titania material would appear to be consistent with many of the observations for the hierarchically structured aluminas. Once the macropore channels were formed, they would preferentially propagate toward the alkoxide since it would provide the least resistant path for the water to react at the solution/alkoxide interface. The driving force for the flow would be the gradient in water concentration caused by hydrolysis.

As with the annodization process, initiation of the regularly arrayed macroporous pattern is more difficult to discern. Hexagonal arrayed structures are energetically favored, which may be the cause of the resulting macropore pattern as proposed within the microphase-separated region. However, as shown in Table 1, an increase in solvent Reynolds number led to a systematic increase in the MMPD. If the macropore formation was initiated after a permeable shell was formed on the alkoxide droplet, the hydrodynamic conditions in the solvent would not be expected to influence the microphase segregation on the other side of the permeable shell. Although the presence of the nonmacroporous region was seen on many particles containing macropores, some of the particles had macropores that completely transversed the particle as seen in Figure 6d.

Seminal to the proposed formation mechanism is the diffusion of water across the membrane and through the liquid channel to the alkoxide surface. Due to the high hydrolysis rate of the aluminum alkoxide, the water concentration at the interface should be extremely small, leading to a large water concentration gradient from the free solvent to droplet surface. However, this diffusion would need to occur against counterdiffusion of butanol formed in the hydrolysis reaction. It is not clear that the diffusion of water against the counterdiffusional flow of butanol and the resistance of the permeable shell would be sufficiently rapid. Therefore, the proposed mechanism does explain many of the observations, but still appears to leave several outstanding questions.

Conclusions

Hierarchically structured aluminas with bimodal pore distribution on the meso- and macroscale were synthesized

(38) Thompson, G. E.; Woo, G. C. Anodic Films on Aluminum. In *Aqueous Processes and Passive Films*; Scully, J. C., Ed.; Academic Press: London, 1983.
(39) Masuda, H.; Fukuda, K. *Science* **1995**, *268*, 1466.
(40) Jessensky, O.; Müller, F.; Gösele, U. *Appl. Phys. Lett.* **1998**, *72*, 1173.
(41) Wu, H.; Zhang, X.; Hebert, K. R. *J. Electrochem. Soc.* **2000**, *147*, 2126.
(42) Thamida, S. K.; Chang, H.-C. *Chaos* **2002**, *12*, 240.

within a well-characterized parameter space. The parametric synthesis study demonstrated that the pore structure at the two length scales could be independently modified. The use of a surfactant was found to influence the mesoscale structure, but not the macroscale structure as long as the synthesis was performed at the same hydrodynamic conditions. The formation of the macroporous structure was found to depend strongly on the hydrodynamic conditions in the synthesis mixture as well as the presence of an aluminum alkoxide droplet in the synthesis mixture. A previously proposed formation mechanism described many, but not all of the features seen in the synthesis study, suggesting that the precise mechanism underlying these hierarchical aluminas remains elusive.

Acknowledgment. Partial support of this research was through the donors of the American Chemical Society Petroleum Research Fund.

CM050315J